Spectroscopic, Structural, and Functional Characterization of the Alternative Low-Spin State of Horse Heart Cytochrome *c*

Katia C. U. Mugnol,* Rômulo A. Ando,[§] Rafael Y. Nagayasu,* Adelaide Faljoni-Alario,[‡] Sergio Brochsztain,* Paulo S. Santos,[§] Otaciro R. Nascimento,[†] and Iseli L. Nantes*

*Centro Interdisciplinar de Investigação Bioquímica (CIIB), Prédio I, Universidade de Mogi das Cruzes (UMC), CP 411, Mogi das Cruzes, SP, CEP 08780-911, Brazil; [†]Instituto de Física de São Carlos, Universidade de São Paulo–São Carlos, CP 369, São Carlos, SP, CEP 13560-970, Brazil; [‡]Departamento de Bioquímica, Instituto de Química, Universidade de São Paulo, CP 26077, São Paulo, CEP 055089-900, Brazil; and [§]Departamento de Química Fundamental, Instituto de Química, Universidade de São Paulo, CP 26077, São Paulo, CEP 055089-900, Brazil

ABSTRACT   The alternative low-spin states of Fe^{3+} and Fe^{2+} cytochrome *c* induced by SDS or AOT/hexane reverse micelles exhibited the heme group in a less rhombic symmetry and were characterized by electron paramagnetic resonance, UV-visible, CD, magnetic CD, fluorescence, and Raman resonance. Consistent with the replacement of Met^{80} by another strong field ligand at the sixth heme iron coordination position, Fe^{3+} ALSScyt*c* exhibited 1-nm Soret band blue shift and ε enhancement accompanied by disappearance of the 695-nm charge transfer band. The Raman resonance, CD, and magnetic CD spectra of Fe^{3+} and Fe^{2+} ALSScyt*c* exhibited significant changes suggestive of alterations in the heme iron microenvironment and conformation and should not be assigned to unfold because the Trp^{59} fluorescence remained quenched by the neighboring heme group. ALSScyt*c* was obtained with His^{33} and His^{26} carboxyethoxylated horse cytochrome *c* and with tuna cytochrome *c* (His^{33} replaced by Asn) pointing out Lys^{79} as the probable heme iron ligand. Fe^{3+} ALSScyt*c* retained the capacity to cleave *tert*-butylhydroperoxide and to be reduced by dithiothreitol and diphenylacetaldehyde but not by ascorbate. Compatible with a more open heme crevice, ALSScyt*c* exhibited a redox potential ~200 mV lower than the wild-type protein (+220 mV) and was more susceptible to the attack of free radicals.

INTRODUCTION

Cytochrome *c* is a hemeprotein peripherally located on the external side of the inner mitochondrial membrane. Cytochrome *c* is a mobile electron carrier of the respiratory chain that, in response to specific signals, can detach from the inner mitochondrial membrane and trigger apoptosis in cytosol (1,2).

In the native form, cytochrome *c* heme iron is hexacoordinated, the fifth and sixth ligands being provided by histidine 18 and methionine 80, respectively. Because the methionine sulfur is a strong field ligand, in the native form, cytochrome *c* heme iron is in the low-spin state. However, the heme iron-sulfur bond can be weakened and broken by either alterations in the microenvironmental conditions or the presence of an alternate ligand (3). As expected, changes in the heme iron sixth ligand affect both cytochrome *c* structure and function.

Among the microenvironmental changes that are able to affect the heme iron distal coordination, the interaction with lipid bilayers has been studied extensively (3–5). Because they are able to affect the sixth coordination position and symmetry of the heme iron, negatively charged membranes strongly influence cytochrome *c* oxidase/peroxidase activity on several substrates, including *tert*-butylhydroperoxide, diphenylacetaldehyde, and methylacetoacetone. The binding of cytochrome *c* to phospholipid bilayers encompasses electrostatic and hydrophobic interactions (3,6). In this regard, Rytömaa and Kinnunen (7–9) proposed a model for the interaction between cytochrome *c* and lipid bilayers that has been reinforced by subsequent studies. In this model, one phospholipid chain is accommodated in a hydrophobic channel present in the cytochrome *c* structure, in the region of the heme crevice. The authors proposed that this might be a common attachment mechanism for peripheral protein/membrane association. In accordance with this model, a clear correlation between the nature of the lipid acyl chain and the spin states of cytochrome *c* interacting with different types of lipid membranes was demonstrated. According to the lipid acyl chain type and the head group charge present in the bilayer, three spin states of cytochrome *c* were observed in different proportions: the native cytochrome *c* low-spin state with rhombic symmetry (spin ½, $g_\perp = 3.07$ and $g_\perp = 2.23$), the high-spin state (spin 5/2, $g_\perp = 6.0$ and $g_\perp = 2.0$), and a low-spin state with less rhombic symmetry (spin ½, $g_1 = 2.902$, $g_2 = 2.225$, and $g_3 = 1.510$ (3)). The latter cytochrome *c* species was named alternative low-spin species or

ALSScyt*c*. The proportion of spin states of cytochrome *c* bound to lipid bilayers at pH 7.4 is also dependent on the lipid/protein ratio, suggesting the existence of two or more protein sites interacting with the lipids. In this regard, we demonstrated that in addition to the lipid-interacting site at pH 7.4 described by Kinnunen and co-workers (site A) (6,7,10), cytochrome *c* also exhibits a pH-regulated site encompassing histidine 26 and 33 and lysines 22, 25, and 27 (site L) (11). With micelles used as membrane models, the literature has also mentioned that the association of cytochrome *c* with SDS micelles leads heme iron to a different low-spin state, probably to the alternative low-spin state, and the increase of the surfactant concentration changes the protein to the high-spin form (12).

The spectroscopic characteristics of both native and high-spin states of cytochrome *c* have been very well characterized. However, to date there is a lack in the literature regarding the spectroscopic and functional characterization of the cytochrome *c* low-spin state with less rhombic symmetry, the ALSScyt*c*. The spectral and functional characterization of ALSScyt*c* is of great interest because CL, present in the inner mitochondrial membrane, could induce this spin state in mitochondria (5). In this study, for the first time, we describe the EPR, UV-visible, CD, MCD, fluorescence, and RR spectral characteristics of the Fe^{3+} and Fe^{2+} ALSScyt*c* as well as the reactivity of this cytochrome *c* species.

MATERIALS AND METHODS

Chemical reagents

Reagents used included horse heart cytochrome *c*, ascorbic acid, DTT, *t*-BuOOH, DEPC. and SDS from Sigma Chemical (St. Louis, MO); ethanolic solution of DPAA and aerosol AOT (Aldrich, Milwaukee, WI); and hexane (P.A.) (Qeel, São Paulo, SP/Brazil). All reagents were of analytical grade.

Preparation of Fe^{2+} cytochrome *c* solutions

Fe^{3+} cytochrome *c* was reduced by a 10-fold excess of ascorbic acid. The reducing agent was removed by the centrifugal filter device Centricon (Millipore, Billerica, MA). The final concentrated cytochrome *c* solution was stored under argon atmosphere to prevent heme iron reoxidation.

SDS-induced ALSScyt*c* solutions

ALSScyt*c* was induced by the addition of 100 μM Fe^{3+} or Fe^{2+} native cytochrome *c* to 7 mM SDS buffered at pH 8.5 by 200 mM TRIS solution. The SDS concentration was chosen from a previous titration of the protein with the surfactant.

AOT/hexane reverse micelle-induced ALSScyt*c*

Cytochrome *c*-containing AOT/hexane reverse micelles were prepared by the addition of 1 ml 200 mM TRIS buffer solution, pH 8.5, containing 1 mM Fe^{3+} or Fe^{2+} cytochrome *c* in 9 ml 0.2 M AOT hexane solution. The mixture was submitted to vortex stirring for 2 min and allowed to rest for 5 min. After stirring, the surfactant molecules assemble so that their heads are in contact with water pools containing cytochrome *c* and their tails are immersed in hexane. The AOT/hexane solution and TRIS-buffered aqueous cytochrome *c* solution ratio should be 10:1 to form a water pool larger than 1.0 nm (13).

Eletronic absorption measurements

UV-visible spectra were obtained in a photodiode spectrophotometer (Multispec 1501, Shimadzu Scientific Instruments, Columbia, MD), using quartz cuvettes with 1.0- and 0.1-cm optical path and 0.5 nm slit.

EPR measurements

The EPR measurements were carried out using an EPR Bruker (Oxford, UK) system, ELEXSYS E-580 model, equipped with a helium cryostat and temperature controller under the following conditions: central field, 2400 G; scanning field, 4000 G; number of points, 2048; modulation amplitude, 10 mT; gain, 45 dB; temperature, 11 K; time constant, 20.48 ms; convertion time, 81.92 ms; microwave power, 8 mW. After the addition of cytochrome *c* in different media, 120 μl of the mixture was quickly introduced into an EPR quartz tube, cooled in liquid nitrogen, and transferred to the helium cryostat and into the EPR cavity to obtain the spectra.

CD and MCD measurements and analysis

The CD and MCD measurements were carried out in a Jasco J-720 spectropolarimeter (Easton, MD) using quartz cuvettes of 0.1-cm optical path; band width, 1.0 nm; scanning speed, 200 nm/min; response, 0.25 s; accumulations, 8.0. For the MCD measurements, the magnetic field was 860 mT. Cytochrome *c* Fe^{2+} samples were prepared and kept in nitrogen atmosphere during handling and analysis.

The spectral deconvolutions (see Fig. 8, *inset*) were obtained by tentative multiplications of native cytochrome *c* MCD spectrum by a factor (Faraday term B), subtraction of obtained Faraday term B for MCD spectrum of ALSScyt*c* (Faraday term A) followed by addition of both obtained terms to result in a MCD spectrum that matched the experimental MCD spectrum of ALSScyt*c*. The best factor obtained to reproduce the experimental MCD spectrum was 2.3.

RR measurements

The RR measurements were obtained at room temperature with laser excitation from the 406.7-nm line of a Kr^+ laser (coherent). The back-scattered light from a slowly rotating NMR tube was collected and focused into a computer-controlled double monochromator (Jobin Yvon U 1000 instrument, Edison, NJ) equipped with a cooled photomultiplier (RCA C31034A-02) and photon-counting electronics. RR spectra were calibrated to 2.0 cm^{-1} accuracy for intense isolated bands with indene as the standard for the high-frequency region and with indene and CCl_4 for the low-frequency region. The other parameters were 50 mW power, time adjusted to 1.0 s, and ranged from 200 to 1800 Rcm^{-1}.

Carboxyethoxylation of cytochrome *c* by DEPC

Samples of 100 μM cytochrome *c* in 10 mM acetate buffer, pH 6.5, were made to react with 15-fold molar excess DEPC at room temperature for 1 min. The samples were dialyzed for 2 h before being subjected to MALDI-TOF mass spectrometer analysis.

MALDI-TOF mass spectrometry

All linear, reflectron (not shown), and postsource decay (not shown) spectra were acquired on an Ettan MALDI-TOF Pro mass spectrometer (GE Healthcare, Chalfont St. Giles, Buckinghamshire, United Kingdom) that can

operate in linear mode or in reflectron mode using a harmonic reflectron that increases resolution and sharpens time focusing. The accelerating voltage was set at 20 kV. The samples were mixed with an equal volume of a saturated solution (5 mg/ml) of 3,5-dimethoxy-4-hydroxycinnamin acid in 50% acetonitrile and 0.5% trifluoroacetic acid, and 0.5 μl of the mixture was loaded onto the stainless steel MALDI slides for analysis.

Fluorescence spectra measurements

Tryptophan fluorescence measurements were carried out in a Fluorescence Spectrophotometer F-2500 (Hitachi, Singapore) at room temperature using excitation at 292 nm; slit, 10.0 nm; scan range, 300 to 400 nm.

Cyclic voltammetry measurements

SAM-modified gold electrodes were prepared using gold-coated glass slides purchased from EMF (Ithaca, NY). The slides were cleaned by immersion in HNO_3 for 2 h, then rinsed copiously with water and dried with argon. The clean gold slides were then incubated with a 10 mM aqueous solution of cystamine dihydrochloride (Aldrich) for 24 h at room temperature, then rinsed with water and dried with an argon flow. Cyclic voltammetry was performed with an AUTOLAB (Herisau, Switzerland) PGSTAT30 potentiostat. All measurements were carried out at 20 ± 2°C in a three-electrode cell consisting of the SAM-modified gold slide as the working electrode (A = 0.25 cm^2), a platinum auxiliary electrode, and an Ag/AgCl reference electrode in 3 M KCl solution. All solutions were purged with argon for 5 min before measurement to remove dissolved oxygen. The measurements in the presence and in the absence of SDS were taken with [cyt c] = 1 mM, using 200 mM TRIS buffer (pH = 8.0) as the support electrolyte. Voltammograms were recorded at a scan rate of 100 mV/s.

RESULTS AND DISCUSSION

EPR spectra of the ALSScyt$c$ Fe^{3+} induced by aqueous and reverse micelles

Fig. 1 shows the EPR spectrum of native low-spin-state cytochrome c with rhombic symmetry (spin ½, g_1 = 3.07, and g_2 = 2.23) obtained in 200 mM TRIS buffer, pH 8.5 (*line a*). In TRIS-buffered AOT/hexane reverse micelles (*line b*) and
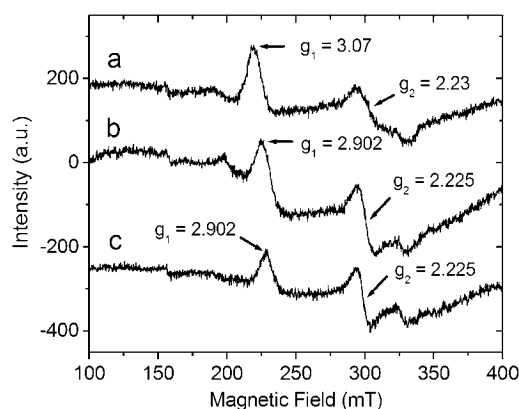

FIGURE 1 EPR spectra of 100 μM low-spin state cytochrome c Fe^{3+} with rhombic symmetry (native form) in 200 mM TRIS buffer, pH 8.5 (*line a*) and 100 μM low-spin-state cytochrome c Fe^{3+} with less rhombic symmetry (ALSScyt$c$) induced by 0.2 M AOT/hexane reverse micelles (*line b*) and by 7.0 mM SDS aqueous micelles (*line c*). Reverse and aqueous micelles were buffered with 200 mM TRIS buffer, pH 8.5.

SDS aqueous micelles (*line c*), cytochrome c was converted to the alternative low-spin form (spin ½, g_1 = 2.902, g_2 = 2.225, and g_3 = 1.510). Partial conversion of cytochrome c to the alternative low-spin form had been previously observed in the presence of cardiolipin and DCP vesicles (3,5).

Characteristics of UV-visible, CD, and MCD spectra of Fe^{3+} ALSScyt$c$ induced by AOT/hexane reverse micelles

Because AOT/hexane reversed micelles and aqueous SDS micelles are able to convert native cytochrome c to the alternative low-spin species, these conditions were used to determine the UV-visible, CD, and MCD spectral characteristics of ALSScyt$c$. Fig. 2 *A* shows the changes in the electronic absorption spectrum (260–760 nm) of Fe^{3+} cytochrome c induced by 7 mM SDS. In this condition, cytochrome c exhibits spectral characteristics attributed to the alternative low-spin form, i.e., 1 nm Soret band blue shift and ε enhancement accompanied by disappearance of the 695-nm charge transfer band. Fig. 2 *B* shows changes in cytochrome c Soret band λ_{max} promoted by increasing SDS concentrations. In 200 mM TRIS buffer, pH 8.5, ALSScyt$c$ spectral features were observed at a SDS concentration range from 1 to 7 mM. With increasing SDS concentration, progressive Soret band blue shift was observed up to the minimal value of 399 nm, observed above 20 mM surfactant and assigned to conversion of native cytochrome c to the high-spin form (UV-visible spectrum not shown). At 200 mM ionic strength, 1 mM SDS was above the critical micellar concentration, and the effect of different SDS concentrations can be rationalized by the model described below. At micelle/cytochrome c ratios ≤1, cytochrome c molecules interact with SDS micelles in such a way that only one face of a cytochrome c molecule contacts a micelle. At micelle/cytochrome c ratios ≥3, cytochrome c surface should be partially covered by SDS micelles, leading to more drastic structural alterations. This model is sketched in Fig. 2 *B*, in which cytochrome c is represented by large gray spheres, SDS micelles by small gray spheres, and the flattening of the large gray sphere represents cytochrome c structural changes. Fig. 2 *C* shows the electronic absorption spectrum of AOT/hexane reverse micelle-induced Fe^{3+} ALSScyt$c$. The similarity of the reverse micelle-induced ALSScyt$c$ electronic absorption spectrum to that observed for the same species obtained in SDS micelles is evident. The spectral characteristics are summarized in Table 1.

At the 260- to 300-nm region of the electronic absorption spectrum carried out in TRIS buffer and in AOT/hexane reverse micelles, a band peaking at 280 nm that could be assigned to the aromatic residues (tyrosine and tryptophan) of the protein can be observed. The same maximal λ and molar extinction coefficient (ε = 0.26 × 10^5 M^{-1}·cm^{-1}) for the 280-nm band was observed for the native and the alternative low-spin forms of cytochrome c. This result suggests that the conditions responsible for the changes in the heme iron
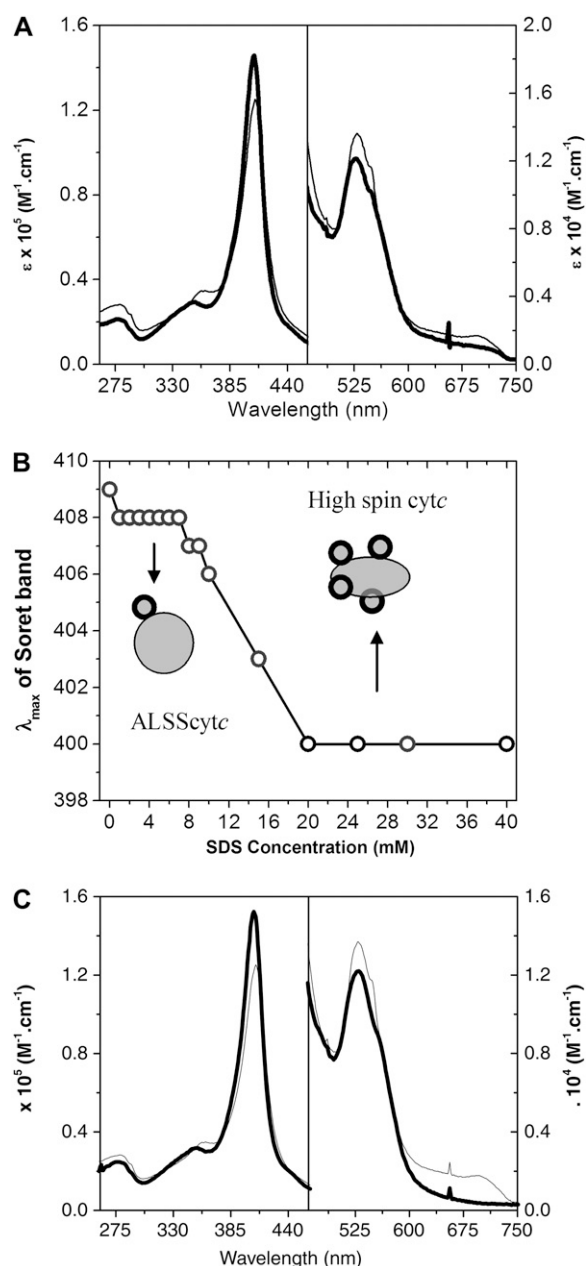
FIGURE 2 (A) Electronic absorption spectrum of 100 μM native Fe^{3+} cytochrome c in 200 mM TRIS buffer, pH 8.5 (*thin solid line*), and 100 μM Fe^{3+} ALSScytc induced by 7.0 mM SDS (*thick solid line*). (B) Blue shift of Soret band λ_{max} as a function of SDS concentration and sketch of cytochrome c interaction with SDS micelles in the concentration range indicated by the arrow. In the sketch, cytochrome c is represented by large gray spheres and SDS micelles by small gray spheres. (C) Electronic absorption spectrum of 100 μM Fe^{3+} native cytochrome c in 200 mM TRIS buffer, pH 8.5 (*thin solid line*) and 100 μM Fe^{3+} ALSScytc induced by 0.2 M AOT/hexane reverse micelles (*thick solid lines*).

TABLE 1 Electronic absorption spectral features of Fe^{3+} cytochrome c in the native and alternative low-spin forms

Electronic absorption bands	Fe^{3+} native cytc		Fe^{3+} ALSScytc	
	λ_{max} (nm)	ε ($M^{-1}cm^{-1}$)	λ_{max} (nm)	ε ($M^{-1}cm^{-1}$)
N	362	0.35×10^5	352	0.32×10^5
Soret	409	1.2×10^5	408	1.5×10^5
Q	529	1.3×10^4	530	1.2×10^4
CT	695	1.8×10^3	–	–

This result can be assigned to changes in the heme iron sphere coordination. The ALSScytc also exhibits significant differences in the Soret band. In the alternative low-spin form, Soret band ε enhanced from 1.25×10^5 $M^{-1}\cdot cm^{-1}$ to 1.52×10^5 $M^{-1}\cdot cm^{-1}$, and Soret band λ_{max} shifted from 409 to 408 nm. These results are also in accordance with changes in the heme iron sphere coordination that result from the weakening of the bond between Met^{80} and the heme iron. Conversion of cytochrome c to the alternative low-spin form did not produce significant changes in Q band λ_{max} and ε values (Table 1).

Conversion of native cytochrome c to the alternative low-spin form produces the disappearance of the charge transfer band (695 nm) assigned to the absence of Met^{80} at the sixth coordination position of heme iron (14). However, in the alternative low-spin state, cytochrome c heme iron should remain hexacoordinated because the complete disruption of this coordination, for example at pH below 3.0 (not shown) or in the presence of high SDS concentrations (Fig. 2 B), promotes a more intense hypsochromic effect leading the Soret to peak at 399 nm (3). The comparison of Fig. 2 A with Fig. 2 B shows that both AOT/hexane reverse micelles and SDS produce identical changes in the cytochrome c electronic absorption spectra. However, in the presence of SDS aqueous micelles, the charge transfer band was not completely abolished. This result could be attributed to the partition of cytochrome c between micelle surface and bulk water, an event that is not expected in the presence of reverse micelles because of space hindrance. This hypothesis is corroborated by the Soret band extinction molar coefficient (ε), which is slightly higher in the presence of AOT/hexane reverse micelles (1.075-fold) than in the presence of SDS micelles.

Striking changes were observed in cytochrome c CD spectra after heme iron conversion to the alternative low-spin form (Fig. 3).

CD spectral features of native and alternative low-spin states of Fe^{3+} cytochrome c are detailed in Table 2. In the region of N band, the CD spectrum of Fe^{3+} cytochrome c exhibits two negative bands (peaks at 330 and 374 nm) that are blue-shifted in the spectrum of the alternative low-spin form (peaks at 326 and 347 nm). This result, as well as the corresponding electronic absorption spectra (Fig. 2 A), suggests changes in the sixth ligand of the heme iron (15).

The native Fe^{3+} cytochrome c CD spectrum (Fig. 3, *thin solid line*) exhibits a Cotton effect (two CD bands of opposite

symmetry did not induce significant alterations in the protein tertiary structure. However, conversion of native cytochrome c to the alternative low-spin form led to a hypsochromic shift (362 to 352 nm) and a slight decrease in the ε value (0.347×10^5 $M^{-1}\cdot cm^{-1}$ to 0.318×10^5 $M^{-1}\cdot cm^{-1}$) of the N-band.
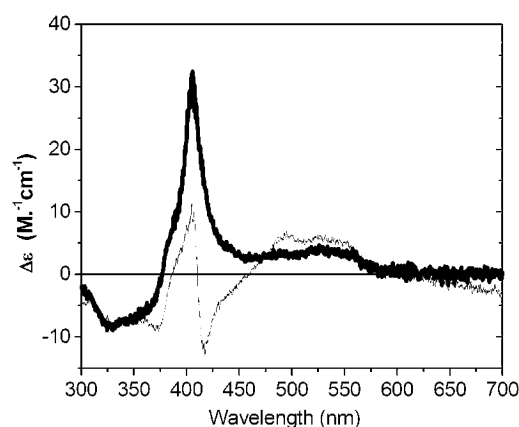
FIGURE 3 CD spectra of 100 μM cytochrome c Fe^{3+} native form in 200 mM TRIS buffer, pH 8.5 (*thin solid line*), and 100 μM cytochrome c Fe^{3+} ALSScyt$c$ in 0.2 M AOT/hexane reverse micelles (*thick solid line*).

sign that are split slightly in energy) in the Soret band with the zero crossing located close to the electronic absorption maximum. The Cotton effect disappeared in the presence of AOT/hexane reverse micelles (Fig. 3, *thick solid line*) because only a broader positive band peaking at 406 nm ($\Delta\varepsilon = 32.27$ $M^{-1}\cdot cm^{-1}$) could be observed in this condition. The weak spectral features in the region between the Soret and Q bands (450–520) have been assigned to charge transfer transitions between the porphyrin and heme iron and are thus sensitive to changes in the axial ligands (16,17). CD visible bands of Fe^{3+} ALSScyt$c$ are also blue-shifted relative to the native form (Fig. 2 and Table 2). Fe^{3+} ALSScyt$c$ exhibits the weak 496- and 540-nm bands blue-shifted to 488 and 530 nm, respectively.

The significant changes in the cytochrome c CD spectrum after the conversion of the heme iron to the alternative low-spin state are suggestive of alterations in the heme iron microenvironment and conformation (16). Particularly, the negative band around 420 nm has been related to the presence of Met[80] at the sixth coordination position of the cytochrome c heme iron (17). Thus, CD results obtained for the cytochrome c alternative low-spin state are in accordance with the loss of the charge transfer band observed in the corresponding electronic absorption spectrum. Similar features were

observed in CD spectrum of Fe^{3+} cytochrome c in the alternative low-spin form obtained by the association with SDS micelles (not shown).

MCD spectra of native and alternative low-spin states of Fe^{3+} cytochrome c are shown in Fig. 4, *A* and *B* (*thin* and *thick solid lines*, respectively), and the peaks and zero crossings are detailed in Table 3. Both native and alternative low-spin forms of Fe^{3+} cytochrome c exhibit symmetrical ''S''-shaped bands in the Soret region with the zero crossing matched closely with the electronic absorption maximum. The ''S''-shaped MCD Soret band arises from the contribution of the Faraday A term. The similarity between the spectra of cytochrome c in the native and alternative low-spin form was expected because MCD is particularly sensitive to the spin state of the heme iron. Literature data have shown that the MCD bands at the Soret region are temperature dependent and are composed of C terms arising from the coupling of the degenerate spin states of paramagnetic, low-spin (spin ½) iron III with the porphyrin $\pi-\pi^*$ transitions (18). AOT/hexane reversed micelles promoted blue shift and $\Delta\varepsilon$
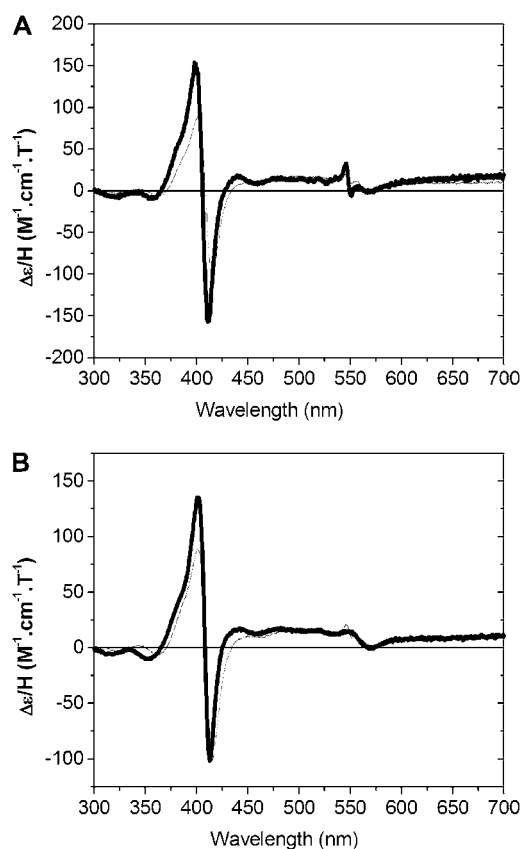
TABLE 2 CD spectral features of Fe^{3+} cytochrome c in the native and alternative low-spin forms

Fe^{3+} native cyt$c$		Fe^{3+} ALSScyt$c$	
λ (nm)	$\Delta\varepsilon$ ($M^{-1}cm^{-1}$)	λ (nm)	$\Delta\varepsilon$ ($M^{-1}cm^{-1}$)
330	−8.05	326	−8.18
374	−9.26	347	−6.71
405	11.3	406	32.27
410	0	–	–
416	−11.6	–	–
496	5.92	488	3.70
540	5.82	530	3.89

FIGURE 4 MCD spectra of Fe^{3+} native and alternative low-spin state cytochrome c. (*A*) MCD spectra of 100 μM cytochrome c Fe^{3+} native form in 200 mM TRIS buffer, pH 8.5 (*thin solid line*), and 100 μM cytochrome c Fe^{3+} ALSScyt$c$ in 0.2 M AOT/hexane reverse micelles (*thick solid line*). (*B*) MCD spectra of 100 μM cytochrome c Fe^{3+} native form in 200 mM TRIS buffer, pH 8.5 (*thin solid line*), and 100 μM Fe^{3+} ALSScyt$c$ in 7.0 mM SDS buffered by 5.0 mM phosphate, pH 7.4 (*thick solid line*).

TABLE 3 MCD spectral features of Fe^{3+} cytochrome *c* in the native and alternative low-spin forms

Fe³⁺ native cyt*c*		Fe³⁺ ALSScyt*c**	
λ (nm)	$\Delta\varepsilon/H$ ($M^{-1}cm^{-1}T^{-1}$)	λ (nm)	$\Delta\varepsilon/H$ ($M^{-1}cm^{-1}T^{-1}$)
322	−3.02	319 (317)	−5.97 (−5.60)
362	−6.34	356 (353)	−7.67 (−9.88)
401	88.85	400 (401)	152.30 (135.34)
408	0	406 (407)	0
415	−100.51	411 (413)	−151.45 (−101.75)
–	–	546 (548)	33.04 (12.62)
549	10.445	550 (560)	0
557	11.01	558[†]	−5.88[†]
570	−1.61	568 (570)	−1.76 (−0.06)

*The values in parentheses were obtained in SDS micelles.
[†]Band absent in SDS micelles.

enhancement of the positive and negative maximal λ in the Soret region as well as the 2-nm blue shift of the zero crossing (Fig. 4 *A*).

The AOT/hexane-induced conversion of native Fe^{3+} cytochrome *c* to the alternative low-spin form also promoted changes in the near-UV, Soret, and Q bands (Fig. 4 *A* and Table 3). As shown before, the UV-visible (Fig. 2 *B*) and CD (not shown) spectral characteristics of Fe^{3+} cytochrome *c* alternative low-spin state obtained in SDS micelles revealed subtle differences relative to the spectra obtained in AOT/ hexane. In particular, the reminiscent charge transfer band detectable in SDS micelles suggested that this medium allows the permanence of a small amount of cytochrome *c* with Met[80] at the sixth coordination position of the heme iron. This proposition was strongly reinforced by the results of MCD. Particularly for the negative component of the MCD band at the Soret region related to the presence of Met[80] at the sixth coordination position, the degree of blue shift and $\Delta\varepsilon$ enhancement were significantly lower (Fig. 4 *B* and Table 3). The contribution of the different microenvironments for the spectral differences should also be considered.

The results described above suggest that Fe^{3+} cytochrome *c* in the alternative low-spin state exhibits Met[80] replaced by another strong field ligand of the heme iron, probably Lys[79]. The RR spectrum of heme proteins has been used to provide useful information on the porphyrin structure (19–21). In this regard, the Raman spectrum of native cytochrome *c* has been completely assigned. Das et al. (22) compared the Raman spectrum of cytochrome *c* associated with SDS to that of native cytochrome *c* in the high- and low-frequency regions of the spectrum. The authors estimated by a deconvolution procedure that, at pH 7.4, ∼95% of cytochrome *c* molecules were bound to SDS micelles. Similarly to our study, the experimental conditions used by Das et al. (22) resulted in a cytochrome *c*/SDS micelles ratio ∼1. In fact, we obtained similar spectral changes in the high- and low-frequency regions of the spectrum of Fe^{3+} cytochrome *c* in the alternative low-spin state. Fig. 5 *A* compares Soret band RR spectra in the region of the high-frequency porphyrin skeletal modes for
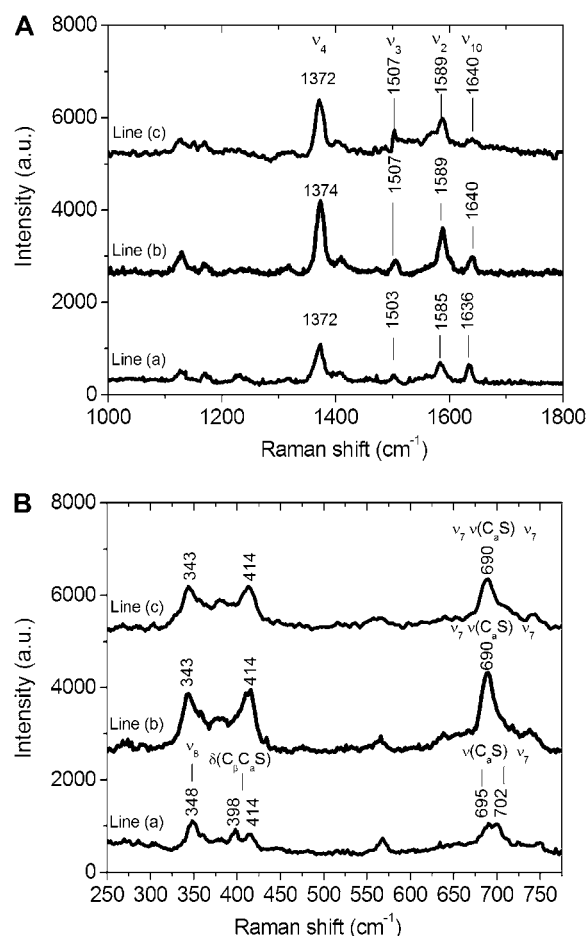

FIGURE 5 RR spectra of native cytochrome *c*, ALSScyt*c*, and high-spin-state cytochrome *c*. (*A*) High-frequency region. (*B*) Low-frequency region. For both panels *A* and *B*, RR spectra of 100 μM cytochrome *c* Fe^{3+} native form in 200 mM TRIS buffer, pH 8.5 (*line a*), of 100 μM cytochrome *c* Fe^{3+} ALSScyt*c* induced by 7.0 mM SDS (*line b*) and 100 μM cytochrome *c* Fe^{3+} high-spin form, induced by 20.0 mM SDS (*line c*).

Fe^{3+} native cytochrome *c* (*line a*), SDS-induced Fe^{3+} cytochrome *c* alternative low-spin form (*line b*), and SDS-induced Fe^{3+} cytochrome *c* high-spin form (*line c*). The labeling of the bands shown in Fig. 5 *A* obeyed the standard mode numbering of octaethylporphyrin and protoheme (23). The skeletal modes ν_{10}, ν_2, and ν_3 are well-characterized markers of porphyrin core size and therefore spin state. The alkaline transition of Fe^{3+} native cytochrome *c* in which Met[80] is replaced by Lys[79] relieves the steric interactions of the thioether ligand with the porphyrin that slightly expand the core size. This phenomenon is responsible for the 2–4 cm^{-1} upshift of the core size marker bands (23). In the case of the SDS-induced ALSScyt*c* (*line b*), ν_{10}, ν_2, and ν_3 are all 4 cm^{-1} upshifted relative to the native form (*line a*) and in accordance with the replacement of Met[80] by Lys[79]. Except for the replacement of Met[80] by Lys[79], it is not expected that other structural similarities could be shared by both ALSScyt*c* and alkaline cytochrome *c*. As sketched in Fig. 2 *B*, ALSScyt*c* should result from the interaction of the

protein with a unique SDS micelle at a specific site leading to structural changes that include the replacement of the heme iron sixth ligand. In this condition, a large extension of protein surface should remain in contact with bulk medium and with the majority of lysine residues protonated. Furthermore, the negatively charged SDS interface is expected to be more acid than the bulk medium and could not create an alkaline microenvironment. The ν_4 band that is a marker of the oxidation state of the porphyrin and only slightly dependent on the core size was 2 cm^{-1} upshifted in the RR spectrum of Fe^{3+} ALSScyt$c$ (line b). For the RR spectrum of SDS-induced high-spin Fe^{3+} cytochrome c, the region of core size marker bands (line c) is noisy and exhibits low-intensity bands, suggesting the presence of reminiscent amounts of cytochrome c in the alternative low-spin form.

Fig. 5 B compares low-frequency spectra of Fe^{3+} native cytochrome c (line a), SDS-induced Fe^{3+} ALSScyt$c$ (line b), and SDS-induced Fe^{3+} cytochrome c high-spin state (line c). The downshift to 690 cm^{-1} observed for the 702 cm^{-1} band, assigned to CS stretching, for the SDS-induced high- and low-spin forms (lines c and b, respectively) reinforces that heme distortion is partially relaxed by the association of the protein with SDS micelles. This assumption is reinforced by the disappearance of the 398 cm^{-1} band (lines b and c) assigned to the bending mode of the sulfur atom of the Cys[14] and Cys[17] residues, the β-carbon of the heme, and the atom bridging these atoms.

Although the RR spectrum of Fe^{3+} ALSScyt$c$ indicated that the surfactant promoted significant changes in the protein tertiary structure, these changes should not be characterized as unfolding because the fluorescence spectrum of Trp[59] was only slightly enhanced (Supplementary Material, Fig. S1, left panel) as compared with the intense fluorescence exhibited by the unfolded corresponding apoprotein (Fig. S1, right panel). Interestingly, the comparison of the normalized fluorescence bands (not shown) indicated that in the alternative low-spin form, the Trp[59] residue is located in a more hydrophobic microenvironment because the fluorescence spectrum, in this condition, was blue-shifted relative to Trp[59] fluorescence of apocytochrome c. This result corroborates that Fe^{3+} ALSScyt$c$ is not unfolded.

Spectral characteristics in UV-visible, CD, and MCD spectra of the Fe^{2+} ALSScyt$c$ induced by AOT/hexane reverse micelles

The Fe^{2+} ALSScyt$c$ was not characterized by EPR because reduced heme iron is EPR silent. However, EPR experiments were conducted in this condition to check the stability of the reduced heme iron in the investigated heterogeneous medium (not shown). The results obtained revealed that cytochrome c alternative low spin remains stable in the reduced form only in AOT/hexane reverse micelles (not shown). Therefore, we characterized the Fe^{2+} cytochrome c alternative low-spin form exclusively in AOT/hexane reverse micelles.

Fig. 6 shows the electronic absorption spectra of ascorbate-reduced Fe^{2+} native cytochrome c (thin solid line) and ascorbate-reduced Fe^{2+} ALSScyt$c$ induced by AOT/hexane reverse micelles (thick solid line). For native Fe^{2+} cytochrome c, the spectral features (Fig. 6, thin solid line) agree with previously published data (24). The electronic absorption spectrum of Fe^{2+} ALSScyt$c$ differs from the native form solely by a 1-nm hypsochromic shift of the Soret band without differences in the visible region. The presence of the Q bands, α and β, in the electronic absorption spectrum of Fe^{2+} ALSScyt$c$ obtained in AOT/hexane indicates that, in this condition, the reduced heme iron presents the sixth coordination position occupied by a strong field ligand (Fig. 6, thick solid line). The high-spin form of Fe^{2+} cytochrome c does not exhibit the Q bands, α and β, and it has been previously characterized for the species produced by the heme iron reduction after exposure of cytochrome c to singlet oxygen (25).

At this point it was important to conduct CD and MCD experiments to characterize the occurrence of significant structural changes in Fe^{2+} ALSScyt$c$.

Fig. 7 shows the CD spectra of Fe^{2+} native cytochrome c (thin solid line) and Fe^{2+} ALSScyt$c$ induced by AOT/hexane reverse micelles (thick solid line). The spectral features are shown in Table 4. The significant differences between the CD spectra of Fe^{2+} cytochrome c in the native and alternative low-spin forms suggest changes in the coordination sphere of the heme iron.

Fig. 8 shows the MCD spectra of Fe^{2+} cytochrome c in the native and alternative low-spin forms (thin and thick solid lines, respectively). The inset shows the calculated MCD spectral contribution for the complex Soret band of the alternative low-spin form. No contribution of the Faraday C terms to the MCD spectrum of reduced porphyrins is expected. The extreme and zero crossings are shown in Table 5. The MCD Soret band of native Fe^{2+} cytochrome c is relatively weak, complex, and does not exhibit a resemblance to the derivative aspect of the absorption spectrum that is ex-
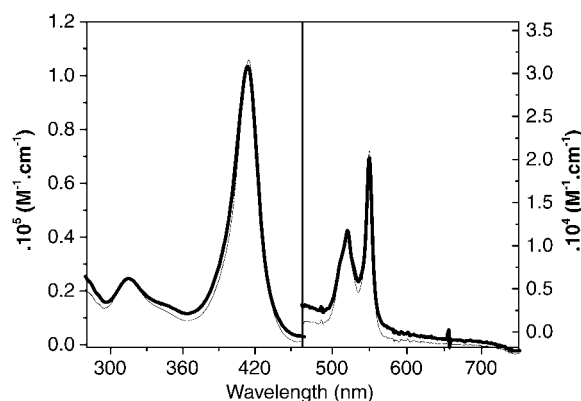
FIGURE 6 Eletronic absorption spectrum of 100 μM ascorbate-reduced Fe^{2+} native cytochrome c in 200 mM TRIS buffer, pH 8.5 (thin solid line), and 100 μM ascorbate-reduced Fe^{2+} cytochrome c in 0.2 M AOT/hexane reverse micelles (thick solid lines).

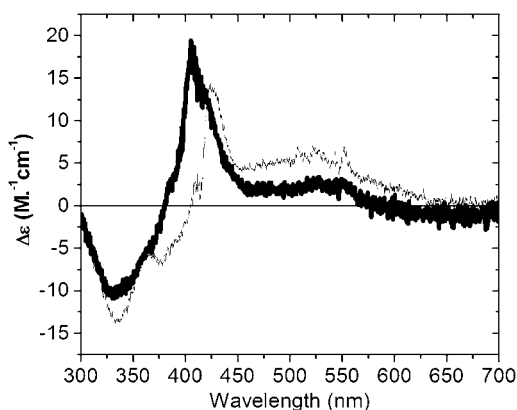FIGURE 7 CD spectra of 100 μM cytochrome *c* Fe^{2+} native form in 200 mM TRIS buffer, pH 8.5 (*thin solid line*), and 100 μM cytochrome *c* Fe^{2+} in 0.2 M AOT/hexane reverse micelles (*thick solid line*).

pected for a Faraday A term. By analogy to cytochromes b_5 and c_3, the complexity of the MCD Soret band suggests the presence of a Faraday B term overlapping the expected A term. A complex MCD spectrum at the Soret band region accompanied the conversion of native Fe^{2+} cytochrome *c* to the alternative low-spin form. The MCD Soret band obtained in this condition suggests a decrease of the Faraday B term contribution. The inset of Fig. 8 shows possible spectral contributions by A and B Faraday terms (*dashed* and *dotted lines*, respectively) resulting in the MCD Soret band of Fe^{2+} ALSScyt*c* (*thick solid line*). In the visible region, both the native and alternative low-spin forms of cytochrome *c* exhibit a relatively intense sigmoidal band with zero crossing at the Q_α absorption band peak (549 nm). In this case, the sigmoidal feature is also assigned to A terms resulting from the degenerate porphyrin electronic excited states. The MCD of the vibrational β band is weak in comparison with the α band because of the overlapping A terms. The only change in the visible region observed in the MCD spectrum of Fe^{2+} ALSScyt*c* is an increase of $\sim$40% in the $\Delta\varepsilon$ of the α and β bands (Table 5).

The heme iron sixth ligand of Fe^{3+} ALSScyt*c*

At this point it was important to have experimental support to assign a cytochrome *c* amino acid residue as the sixth ligand of the heme iron for the protein in the alternative low-spin

TABLE 4 CD spectral features of Fe^{2+} cytochrome *c* in the native and alternative low-spin forms

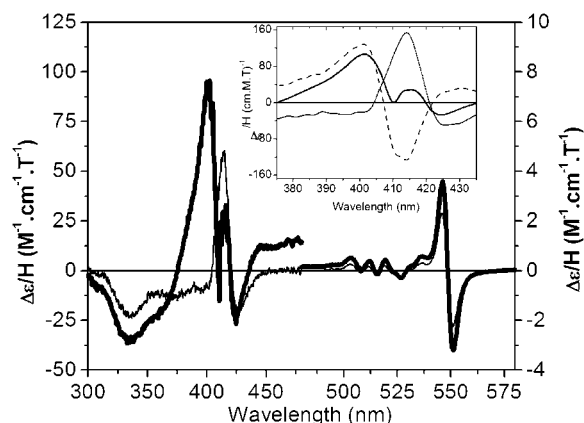|	Fe^{3+} native cyt*c*		Fe^{3+} ALSScyt*c*
λ (nm)	$\Delta\varepsilon$ ($M^{-1}cm^{-1}$)	λ (nm)	$\Delta\varepsilon$ ($M^{-1}cm^{-1}$)
335	−13.50	335	−10.34
405	0	380	0
424	13.66	405.5	19.25
533	5.72	533	2.12

FIGURE 8 MCD spectra of 100 μM cytochrome *c* Fe^{2+} native form in 200 mM TRIS buffer, pH 8.5 (*thin solid line*), and 100 μM cytochrome *c* Fe^{2+} in 0.2 M AOT/hexane reverse micelles (*thick solid lines*). (*Inset*) Calculated MCD spectral contribution to the MCD Soret band of Fe^{2+} ALSScyt*c*. Dotted line (Faraday B term) corresponds to 2.3-fold Fe^{2+} native cytochrome *c* spectrum, and dashed line (Faraday A term) corresponds to Fe^{2+} ALSScyt*c* MCD spectrum minus dotted line data. Thick solid line corresponds to dotted line data (2.3-fold Fe^{2+} native cytochrome *c* spectrum) plus dashed line data (Fe^{2+} ALSScyt*c* MCD spectrum minus 2.3-fold Fe^{2+} native cytochrome *c* spectrum) and matches with the experimental Fe^{2+} cytochrome *c* MCD spectrum.

form. From the analysis of cytochrome *c* structure, Lys[79] arose as the most probable ligand that substitutes for Met[80] when the protein binds on the surface of SDS micelles or is entrapped inside AOT/hexane reverse micelles. However, literature data have also assigned His[33] and His[26] as the probable sixth heme iron ligand when cytochrome *c* is associated to SDS micelles (23,26,27). Thus, the chemical modification of His[33] and His[26] could provide support to the assignment of the sixth heme iron ligand. In the native structure of cytochrome *c*, these histidine residues are superficially localized and prone to be modified by DEPC. According to previous studies in our laboratory, the treatment of cyto-

TABLE 5 MCD spectral features of Fe^{2+} cytochrome *c* in the native and alternative low-spin forms

	Fe^{3+} native cyt*c*		Fe^{3+} ALSScyt*c*
λ (nm)	$\Delta\varepsilon$/H ($M^{-1}cm^{-1}T^{-1}$)	λ (nm)	$\Delta\varepsilon$/H ($M^{-1}cm^{-1}T^{-1}$)
335	−23.49	335	−35.48
		375	0
		402	94.31
404	0	411	0
414	58.71	415	31.60
420	0	420	0
426	−19.78		
530	0	530	0
537	30.64	537	57.67
546	228.99	546	356.64
548	0	549	0
551	−224.28	551	−319.67
568	0	568	0

The β-band values were omitted for clarity.

chrome *c* with DEPC at a pH <6.0 allows superficial histi-
dine residues to be the principal target for carbethoxylation
(12). Cytochrome *c* was treated with DEPC at pH 5.5, dia-
lyzed, and submitted to MALDI-TOF spectral analysis be-
fore and after trypsin digestion to confirm the expected
chemical modification. The carbethoxylated cytochrome *c*
was added to TRIS-buffered pH 8.0 aqueous solution, SDS
micelles, and AOT/hexane reverse micelles. The UV-visible
spectra of carbethoxylated cytochrome *c* associated with
SDS micelles and AOT/hexane reverse micelles were iden-
tical to those obtained with the native protein in the studied
heterogeneous medium (Fig. S2). EPR spectrum of the
carbethoxylated cytochrome *c* both in TRIS buffer and as-
sociated with SDS micelles exhibited the same *g* values of the
corresponding spectra of nonmodified cytochrome *c* (com-
pare Fig. 1, *lines a* and *b*, with Fig. 9, *lines a* and *b*). This
result pointed out that the ALSScyt*c* should not present a
histidine residue at the sixth coordination position of heme
iron. Furthermore, tuna cytochrome *c*, in which the His[33]
residue is replaced by Asp, also exhibited the typical
ALSScyt*c* electronic absorption spectrum when associated
with SDS micelles in 1:1 protein/micelle ratio (not shown)
and exhibited identical reactivity with diphenylacetaldehyde
(Fig. S3) as compared with horse heart cytochrome *c* (see
below).

Reactivity of ALSScyt*c* induced by aqueous and reverse micelles

To estimate changes in the reactivity, we determined, by
cyclic voltammetry, the redox potential of ALSScyt*c* ($\sim +20$
mV versus SHE) that was shifted negatively by 200 mV
relative to the native protein (not shown). This value was
corroborated by the incapacity of ALSScyt*c* to oxidize as-
corbate, whose redox potential is +58 mV (not shown). In
the respiratory chain, as an electron shuttle, cytochrome *c*

FIGURE 9   EPR spectra of 100 μM carbethoxylated Fe^{3+} cytochrome *c* in
200 mM TRIS buffer, pH 8.5 (*line a*), and associated with 7.0 mM SDS
micelles (*line b*).

accepts electrons from Complex III at a redox potential of
$\sim +250$ mV versus SHE and donates electrons to the Cu_A site
in Complex IV at a redox potential of $\sim +285$ mV versus
SHE. Thus, the lowering of 200 mV in the redox potential
precludes the participation of ALSScyt*c* in the electron
transport between complexes III and IV (28). However,
the biological function of cytochrome *c* is not restricted to the
respiratory chain. Cytochrome *c* also participates in the
triggering of cell apoptosis, and this function requires pre-
vious detachment of cytochrome *c* from the inner mito-
chondrial membrane with unavoidable disruption of electron
shuttling (1,2). Recently, Basova et al. (29) reported that
during apoptosis, CL migrates from the inner leaflet to the
outer leaflet of the inner membrane and further to the outer
mitochondrial membrane, setting the stage for its facilitated
interaction with cytochrome *c*. It is postulated that apoptosis-
associated redistribution of CL between the inner and outer
mitochondrial membranes makes CL available for binding
with cytochrome *c* and leads to a negative shift of its redox
potential with consequent conversion of cytochrome *c* into a
peroxidase (30). The authors proposed that the negative shift
of the cytochrome *c* redox potential induced by CL rather
than its physical separation from the mitochondrial com-
plexes is the major mechanism to turn off the electron-
transporting function of cytochrome *c* in the mitochondrial
respiratory chain. In this regard, in model systems, we have
previously observed (5) that CL was able to induce the
conversion of cytochrome *c* from native low-spin form to the
alternative low-spin form. Thus, the apoptosis-associated
increase of CL availability in the outer leaflet of the inner
mitocondrial membrane could lead to the conversion of cy-
tochrome *c* to ALSScyt*c*.

Because of the negative shift of the redox potential ex-
hibited by ALSScyt*c*, it was important to probe its reactivity
with peroxides and aldehydes, which are expected products
of lipid membrane oxidation. Literature data have shown that
even native Fe^{3+} cytochrome *c* exhibits the capacity to cleave
peroxides (4,31) and to oxidize DPAA (32–34), and these
reactions are influenced by the presence of charged inter-
faces. As previously described (4,31), the reaction of cyto-
chrome *c* with *t*-BuOOH leads to Soret band bleaching as
a result of the attack of free radicals (alkoxyl and peroxyl)
on the heme group. In the native form, after addition of
t-BuOOH, cytochrome *c* Soret band bleaching occurred with
a rate of 0.014 min^{-1} (not shown). In the SDS-induced al-
ternative low-spin form, the rate of Soret band bleaching
increased to 0.085 min^{-1} (not shown), suggesting a more
open heme crevice in this condition that made the heme
group more susceptible to free radical attack. Interesting re-
sults were obtained by comparing the reduction of native and
alternative low-spin-state cytochrome *c* by DPAA and DTT.

The reduction of Fe^{3+} native cytochrome by equimolar
amounts of both DPAA (not shown) and DTT (Fig. 10 *A*) led
to well-known changes in the electronic absorption spectrum
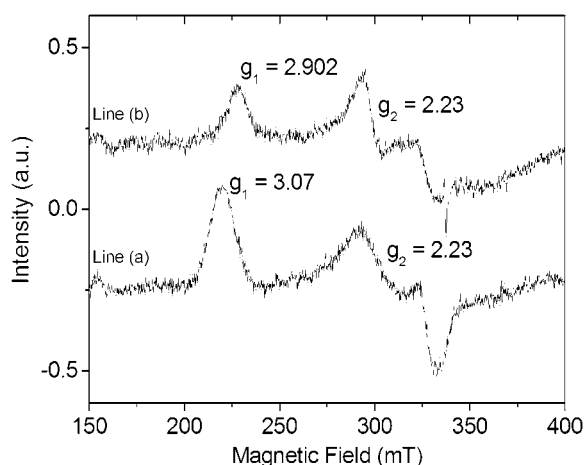(24) compatible with the formation of the Fe^{2+} cytochrome
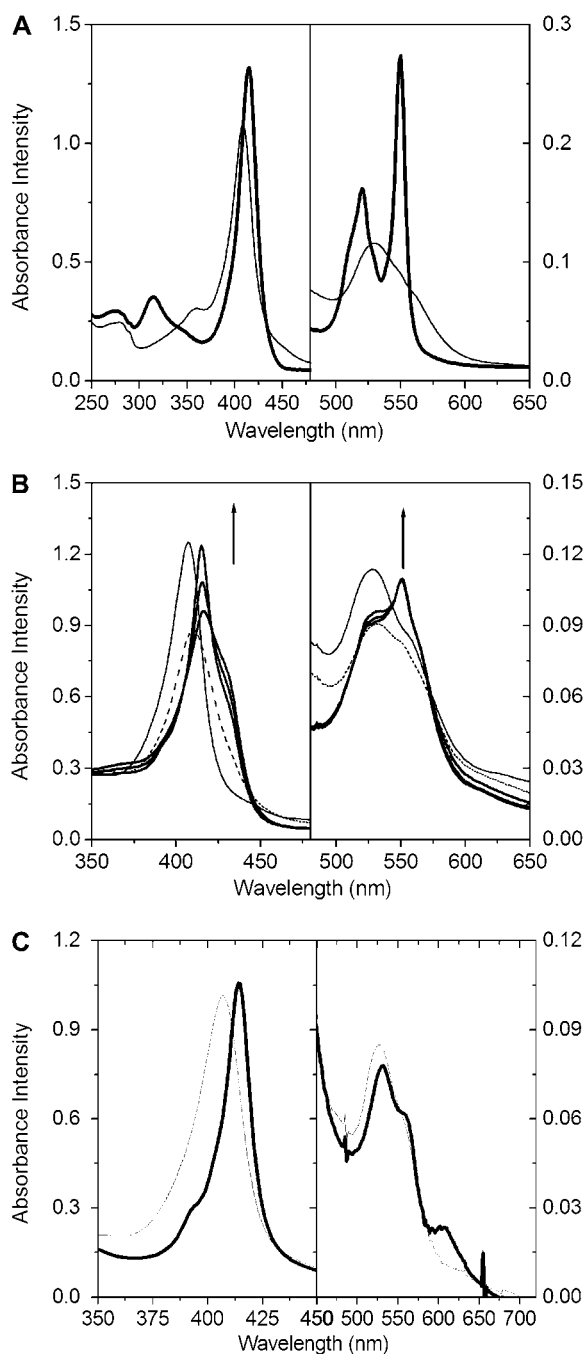
FIGURE 10 (A) Electronic absorption spectrum of 100 μM cytochrome c Fe^{3+} native form in 200 mM TRIS buffer, pH 8.5 (*thin solid line*), and after addition of 100 μM DTT (*thick solid lines*). (B) Time electronic absorption spectrum of 100 μM Fe^{3+} cytochrome c native form in 200 mM TRIS buffer, pH 8.5 (*thin solid line*), and 100 (*dashed line*), 500, 3000, and 7200 s (*thick solid lines*) after addition of 100 μM DTT. (C) Electronic absorption spectrum of 100 μM ALSScytc Fe^{3+} induced by 7.0 mM SDS in 5 mM phosphate buffer, pH 7.4, and after addition of 100 μM DPAA (*thick solid line*).

c in the native low-spin form. As previously described for ascorbate-reduced cytochrome c (Fig. 6), the addition of SDS to Fe^{2+} native cytochrome c that was previously reduced by DPAA or DTT led to the minimal spectral changes that

characterize Fe^{2+} ALSScytc (not shown). However, when the reducing agent was added to the previously formed Fe^{3+} ALSScytc, the spectral changes were significantly different. Fig. 10 B shows the UV-visible spectra of SDS-induced ALSScytc in the course of the reaction with DTT. The spectrum obtained immediately after DTT addition reveals a 3-nm bathochromic shift of the Soret band and ε decrease without significant changes in the visible bands (*dotted line*). This spectrum suggests change in the heme iron ligand preceding the electron transfer. Probably because of a more open heme crevice in ALSScytc, a thiol group of reduced DTT (here represented as HSDTTSH) approaches the heme iron, suffers metal-induced acid dissociation to HSDTTS- and coordinates with the metal. Cytochrome c spectra obtained at subsequent times and indicated by the arrows revealed changes suggestive of low-spin-form cytochrome c reduction. However, in these conditions, Fe^{2+} cytochrome c spectra suggest the presence of a heme iron sixth ligand different from Met[80] or Lys[79], probably a deprotonated thiol group of DTT that remained occupying the heme crevice. Scheme 1 illustrates the mechanistic proposal for Fe^{3+} ALSScytc reduction by DTT, where R1 represents any molecule able to react with -S$^{\bullet}$ produced by the oxidative attack of heme iron. Details about the structure and heme iron ligands of this cytochrome c species remain to be elucidated.

Data from our laboratory demonstrated that the reduction of cytochrome c heme iron by DPAA is dependent on the position and protonation state of two protein tyrosine residues, probably Tyr[67] and Tyr[74] (34). The ALSScytc induced by SDS micelles retained the reactivity with DPAA, corroborating that SDS-bound cytochrome c is not unfolded. However, the SDS-induced ALSScytc exhibits an electronic absorption spectrum compatible with Fe^{2+} high-spin-state cytochrome c because Q band α and β are absent, whereas a 623-nm band is present (25) (Fig. 10 C).

The reduction of native cytochrome c by DPAA probably involves electron transfer via heme edge without displacement of the heme iron ligands. This process permits the reduced protein to be generated in the low-spin state. However, the ALSScytc, probably because it has a more open heme crevice, permits DPAA free radical to attack (Schiff base formation) and displace Lys[79], postulated as the sixth ligand of heme iron. The reduction of ALSScytc was disfavored in AOT/hexane reverse micelles (not shown). In this condition, only Soret band bleaching was observed, indicating the formation of DPAA free radicals from heme iron oxidative attack. Previously, we demonstrated that HRP- and cytochrome c-promoted DPAA oxidation leads to the formation of triplet benzophenone and singlet oxygen (32,33,35). Thus, in this condition, the detection of Fe^{2+} cytochrome c could be impaired by rapid reoxidation promoted by singlet oxygen. As previously described (23), this excited species could also attack the heme group, leading to Soret band bleaching. The high oxygen availability provided by the hexane phase could also allow rapid reaction of O_2 with DPAA$^{\bullet}$ preventing the
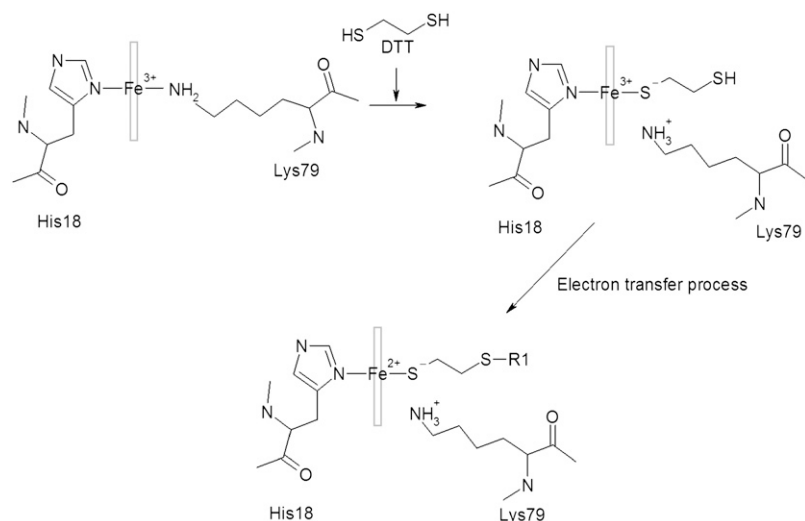
SCHEME 1 Proposed mechanism for Fe^{3+} ALSScyt*c* reduction by DTT.

formation of Lys[79] Schiff base and the conversion of the protein to the high-spin form.

CONCLUSIONS

The results presented above lead to the following conclusions: 1), SDS micelles in equimolar amounts with cytochrome *c* and AOT/hexane reverse micelles convert both Fe^{3+} and Fe^{2+} hemeprotein to the alternative low-spin state; 2), Fe^{3+} ALSScyt*c* exhibits the heme iron with a less rhombic symmetry, probably because of the replacement of Met[80] by Lys[79] at the sixth coordination position. This proposal is based on the capacity of both tuna cytochrome *c* (His[33] replaced by Trp) and His[26] and His[33] carbethoxylated horse cytochrome *c* to be converted to ALSScyt*c* by SDS and AOT/hexane reverse micelles. For Fe^{2+} ALSScyt*c*, the CD and MCD spectral changes reflect significant structural modifications that could or could not be accompanied by replacement of the heme iron sixth ligand; 3), ALSScyt*c* exhibits structural changes and a more open heme crevice relative to the native form; however, in these conditions, the protein is not unfolded because Trp[59] remains close to the heme iron; 4), the reactivity of ALSScyt*c* exhibits peculiarities dictated by the heterogeneous medium, but they are all in accordance with a more open heme crevice; and 5), the spectral and functional characterization of ALSScyt*c* is of great interest because ALSScyt*c* could be found in the inner mitochondria membrane when CL availability is increased by apoptotic stimulus.

SUPPLEMENTARY MATERIAL

To view all of the supplemental files associated with this article, visit www.biophysj.org.

REFERENCES

1. Yang, J., X. S. Liu, K. Bhalla, C. N. Kim, A. M. Ibrado, J. Cai, T. Peng, D. P. Jones, and X. Wang. 1997. Prevention of apoptosis by Bcl-2: release of cytochrome *c* from mitochondria blocked. *Science*. 275:1129–1132.

2. Kluck, R. M., E. Bossy-Wetzel, D. R. Green, and D. D. Newmeyer. 1997. The release of cytochrome *c* from mitochondria: a primary site for Blc-2 regulation of apoptosis. *Science*. 275:1132–1136.

3. Nantes, I. L., M. R. Zuchhi, O. R. Nascimento, and A. Faljoni-Alario. 2001. Effect of heme iron valence state on the conformation of cytochrome *c* and its association with membrane interfaces. *J. Biol. Chem.* 276:153–158.

4. Nantes, I. L., A. Faljoni-Alário, O. R. Nascimento, B. Bandy, R. Gatti, and E. J. H. Bechara. 2000. Modifications in heme iron of free and vesicle bound cytochrome *c* by *tert*-butyl hydroperoxide: a magnetic circular dichroism and electron paramagnetic resonance investigation. *Free Radic. Biol. Med.* 28:786–796.

5. Zucchi, M. R., O. R. Nascimento, A. Faljoni-Alário, T. Prieto, and I. L. Nantes. 2003. Modulation of cytochrome *c* spin states by lipid acyl chains: a continuous-wave electron paramagnetic resonance (CW-EPR) study of haem iron. *Biochem. J.* 370:671–678.

6. Rytömaa, M., and P. K. J. Kinnunen. 1995. Reversibility of the binding of cytochrome *c* to liposomes. *J. Biol. Chem.* 270:3197–3202.

7. Rytömaa, M., and P. K. J. Kinnunen. 1994. Evidence for two distinct acidic phospholipid-binding sites in cytochrome *c*. *J. Biol. Chem.* 269:1770–1774.

8. Tuominen, E. K. J., C. J. A. Wallace, and P. K. J. Kinnunen. 2002. Phospholipid-cytochrome *c* interaction. *J. Biol. Chem.* 277:8822–8826.

9. Tuominen, E. K. J., K. Zhu, C. J. A. Wallace, I. Clark-Lewis, D. B. Craig, M. Rytömaa, and P. K. J. Kinnunen. 2001. ATP induces a conformational change in lipid-bound cytochrome *c*. *J. Biol. Chem.* 276:19356–19362.

10. Rytömaa, M., P. Mustonen, and P. K. J. Kinnunen. 1992. Reversible, nonionic, and pH-dependent association of cytochrome *c* with cardiolipin-phosphatidylcholine liposomes. *J. Biol. Chem.* 267:22243–22248.

11. Kawai, C., F. M. Prado, G. L. C. Nunes, P. Di Mascio, A. M. Carmona-Ribeiro, and I. L. Nantes. 2005. pH-dependent interaction of cytochrome *c* with mitochondrial mimetic membranes. *J. Biol. Chem.* 280:34709–34717.

12. Gebicka, L., and J. L. Gebicki. 1999. Kinetic studies in the interaction of ferricytochrome *c* with anionic surfactants. *J. Protein Chem.* 18:165–172.

13. Birdi, K. S. Handbook of Surface and Colloid Chemistry. 1997. CRC Press, New York. 496–529.

14. Brautigan, D. L., B. A. Feinberg, B. M. Hoffman, E. Margoliash, J. Preisach, and W. E. Blumberg. 1997. Multiple low spin forms of the cytochrome *c* ferrihemochrome. *J. Biol. Chem.* 252:574–582.

15. Riposati, A., T. Prieto, C. S. Shida, I. L. Nantes, and O. R. Nascimento. 2006. Low spin states of microperoxidases produced by inter- and intra-peptide chain sixth ligands: effect of pH and the oligopeptide type. *J. Inorg. Biochem.* 100:226–238.

16. Blauer, G., N. Sreerama, and R. Woody. 1993. Optical activity of hemoproteins in the Soret region. Circular dichroism of the heme undecapeptide of cytochrome *c* in aqueous solution. *Biochemistry.* 32:6674–6679.

17. Santucci, R., and F. Ascoli. 1995. The Soret circular dichroism spectrum as a probe for the heme Fe(III)-Met(80) axial bond in horse cytochrome *c*. *J. Inorg. Biochem.* 270:3197–3292.

18. O'Connor, D. B., R. A. Goldbeck, J. H. Hazzard, D. S. Kliger, and M. A. Cusanovich. 1993. Time-resolved absorption and magnetic circular dichroism spectroscopy of cytochrome c_3 from Desulfobrivio. *Biophys. J.* 65:1718–1726.

19. Sinibaldi, F., B. D. Howes, M. C. Piro, P. Caroppi, G. Mei, F. Ascoli, G. Smulevich, and R. Santucci. 2006. Insights into the role of the histidines in the structure and stability of cytochrome *c*. *J. Biol. Inorg. Chem.* 11:52–62.

20. Caroppi, P., F. Sinibaldi, E. Santoni, B. D. Howes, L. Fiotucci, T. Ferri, F. Ascoli, G. Smulevich, and R. Santucci. 2004. The 40s Ω-loop plays a critical role in the stability and the alkaline conformational transition of cytochrome *c*. *J. Biol. Inorg. Chem.* 9:997–1006.

21. Hu, S., I. K. Morris, J. P. Singh, K. M. Smith, and T. G. Spiro. 1993. Complete assignment of cytochrome *c* resonance raman spectra via enzymatic reconstitution with isotopically labeled hemes. *J. Am. Chem. Soc.* 115:12446–12458.

22. Das, T. K., S. Mazundar, and S. Mitra. 1998. Characterization of a partially unfolded structure of cytochrome *c* induced by sodium dodecyl sulphate and the kinetics of its refolding. *Eur. J. Biochem.* 254:662–670.

23. Smulevich, G., M. J. Bjerrum, H. B. Gray, and T. G. Spiro. 1994. Resonance Raman Spectra and the active site structure of semisynthetic Met80Cys horse heart cytochrome *c*. *Inorg. Chem.* 33:4629–4634.

24. Campos, I. B., I. L. Nantes, F. A. Rodrigues, and S. Brochsztain. 2004. Photoinduced electron transfer in silica-supported self-assembled thin films containing a 1,4,5,8-naphthalenetetracarboxylic diimide and cytochrome *c*. *J. Mater. Chem.* 14:1–8.

25. Estevam, M. L., O. R. Nascimento, M. S. Baptista, P. Di Mascio, F. M. Prado, A. Faljoni-Alário, M. R. Zucchi, and I. L. Nantes. 2004. Changes in the spin state and reactivity of cytochrome *c* induced by photochemically generated-singlet oxygen and free radicals. *J. Biol. Chem.* 279:39214–39222.

26. Yoshimura, T. 1998. A change in the heme stereochemistry of cytochrome *c* upon addition of sodium dodecyl sulfate: electron paramagnetic resonance and electronic absorption spectral study. *Arch. Biochem. Biophys.* 264:450–461.

27. Oellerich, S., H. Wackerbarth, and P. Hildebrandt. 2003. Conformational equilibria and dynamics of cytochrome *c* induced by binding of sodium dodecyl sulfate monomers and micelles. *Eur. Biophys. J.* 32:599–613.

28. Wang, H., D. F. Blair, W. R. Ellis, H. B. Gray, Jr., and S. I. Chan. 1986. Temperature dependence of the reduction potential of CuA in carbon monoxide inhibited cytochrome *c* oxidase. *Biochemistry.* 25:167–171.

29. Basova, L. V., I. V. Kurnikov, L. Wang, V. B. Ritov, N. A. Belikova, I. I. Vlasova, A. A. Pacheco, D. E. Winnica, J. Peterson, H. Bayir, D. H. Waldeck, and V. E. Kagan. 2007. Cardiolipin switch in mitochondria: shutting off the reduction of cytochrome *c* and turning on the peroxidase activity. *Biochemistry.* 46:3423–3434.

30. Fernandez, M. G., L. Troiano, L. Moretti, M. Nasi, M. Pinti, S. Salvioli, J. Dobrucki, and A. Cossarizza. 2002. Early changes in intramitochondrial cardiolipin distribution during apoptosis. *Cell Growth Differ.* 13:449–455.

31. Barr, D. P., and R. P. Mason. 1995. Mechanism of radical production from the reaction of cytochrome *c* with organic hydroperoxides. *J. Biol. Chem.* 270:12709–12716.

32. Nantes, I. L., G. Cilento, and E. J. H. Bechara. 1995. Chemiluminescent diphenylacetaldehyde oxidation by mitochondria is promoted by cytochromes and leads to oxidative injury of the organelle. *Photochem. Photobiol.* 62:522–527.

33. Nantes, I. L., A. Faljoni-Alário, A. E. Vercesi, K. E. Santos, and E. J. Bechara. 1998. Liposome effect on the cytochrome *c*-catalyzed peroxidation of carbonyl substrates to triplet species. *Free Radic. Biol. Med.* 25:546–553.

34. Rinaldi, T. A., I. L. S. Tersariol, F. H. Dyszy, F. M. Prado, O. R. Nascimento, P. Di Mascio, and I. L. Nantes. 2004. Protonation of two adjacent tyrosine residues influences the reduction of cytochrome *c* by diphenylacetaldehyde: a possible mechanism to select the reducer agent of heme iron. *Free Radic. Biol. Med.* 36:802–810.

35. Nantes, I. L., E. J. H. Bechara, and G. Cilento. 1996. Horseradish peroxidase-catalyzed generation of acetophenone and benzophenone in the triplet state. *Photochem. Photobiol.* 63:702–708.